Forced Resonant Oscillations as a Response to Periodic Winds in a Stratified Reservoir

Javier Vidal[1] and Xavier Casamitjana[2]

Abstract: The response of the Sau reservoir to a wind field characterized by having marked periodicities of 12 h and 24 h has been studied. Measurements of temperature, with a thermistor string, and currents, with an acoustic Doppler current meter, show that the reservoir also responds with the same water periodicities. During certain times of the stratified period, some of the natural oscillation modes of the reservoir are close to these forcing wind periods. In particular, in mid-July the vertical Mode V2 is close to 12 h and in mid- to end of September the vertical Mode V3 is close to 24 h. In these situations, these modes are selected out of the spectrum of possible internal waves and the reservoir behaves as a forced oscillator in resonance with the wind. The structure and the period of these vertical modes have been elucidated by using the 3D model ELCOM. Both modes are affected by the Earth's rotation at the widest part of the reservoir.

DOI: 10.1061/(ASCE)0733-9429(2008)134:4(416)

CE Database subject headings: Oscillations; Wind; Reservoirs; Measurement; Temperature.

Introduction

Basin-scale, wind-induced motions depend on interactions of spatially and temporally varying wind forcing with bathymetry, density distribution, and the Earth's rotation (Laval et al. 2003). These motions include wind-driven currents and basin-scale internal waves. Basin internal waves are commonly excited in the following way: Wind stress forces the surface water toward the downwind end of the lake, thus giving rise to a horizontal pressure gradient, which, in turn, accelerates the deeper water toward the upwind end. After the wind forcing relaxes, the metalimnion oscillates, generating a standing internal wave, or seiche. The amplitudes and the periods of these oscillations have been described in numerous studies [see, for example, Spiegel and Imberger (1980), Stevens et al. (1996), and Lemmin et al. (2005)]. Currents and vertical displacements have been shown to affect the spatial distribution of different organisms (Levy et al. 1991; McManus et al. 2005). Internal waves cause a periodic vertical displacement of the suspended biomass and, thus, a periodic variation in the light intensity to which algal cells are exposed (Kamykowski 1979; Gaedke and Schimmele 1991), which in turn influences the rate of photosynthesis (Pahl-Wostl and Imboden 1990). The bottom currents induced by internal waves also contribute to the mixing and resuspension of sediments in the benthic boundary layer by transporting the products of bacterial decomposition away from the sediment-water interface into the bulk water (Gloor et al. 1994). Therefore, an internal wave can play a significant role in governing the vertical structure of water quality.

Internal seiches can be divided into different categories, depending on the nodal lines. In a two-dimensional system, it is usual to represent the modes as: VnHm where n and m are the number of the vertical and horizontal modes (Münnich et al. 1992). Furthermore, horizontal modes can be longitudinal or transversal, depending on the position of the horizontal node line (Lemmin et al. 2005). At large scales, where the Earth's rotation is important, the horizontal nodal lines form amphidromic points. As many lakes can be approximated by a two-layer body (epilimnion and hypolimnion), separated by a narrow interface (metalimnion), the V1 is the most commonly excited mode. However, the presence of a thick metalimnion combined with the resonance between the wind and higher modes can lead to the excitation of these modes. Second vertical modes have been reported by LaZerte (1980), Wiegand and Chamberlain (1987), Münnich et al. (1992), and Roget et al. (1997). Wiegand and Chamberlain (1987) observed that for the case of Wood Lake (British Columbia), with a thick metalimnion, after a wind event, initial excitation of the V1 mode was typically followed by excitation and dominance of the V2 mode. Münnich et al. (1992) showed that the second vertical mode is dominant in the wave field of Alpnacher See, a side basin of Lake Lucerne, and that resonance with diurnal wind is responsible for the large amplitudes of the mode. In Lake Kinneret, the largest internal wave energy response occurred when the natural internal wave frequency was similar to the forcing frequency of the wind. This was shown to occur at two different periodicities: 24 h and 50 h (Antenucci and Imberger 2003).

To our knowledge, the only experimental evidence of a third vertical mode (V3) has been reported in Vidal et al. (2005). In that paper, experimental evidence of a V3 mode with a period of ~24 h occurring in Sau reservoir (Spain) is presented. This mode was found to dominate the internal wave field during the first days of September 2003, when the stratification was fully developed. In addition, a two-dimensional eigenvalue model for the stream

[1]Departament de Física i Institut de Medi Ambient, Universitat de Girona, 17071 Girona, Spain. E-mail: javiervidal@ugr.es

[2]Departament de Física i Institut de Medi Ambient, Universitat de Girona, 17071 Girona, Spain. E-mail: xavier.casamitjana@udg.es

Note. Discussion open until September 1, 2008. Separate discussions must be submitted for individual papers. To extend the closing date by one month, a written request must be filed with the ASCE Managing Editor. The manuscript for this paper was submitted for review and possible publication on May 19, 2006; approved on August 8, 2007. This paper is part of the ***Journal of Hydraulic Engineering***, Vol. 134, No. 4, April 1, 2008. ©ASCE, ISSN 0733-9429/2008/4-416–425/$25.00.

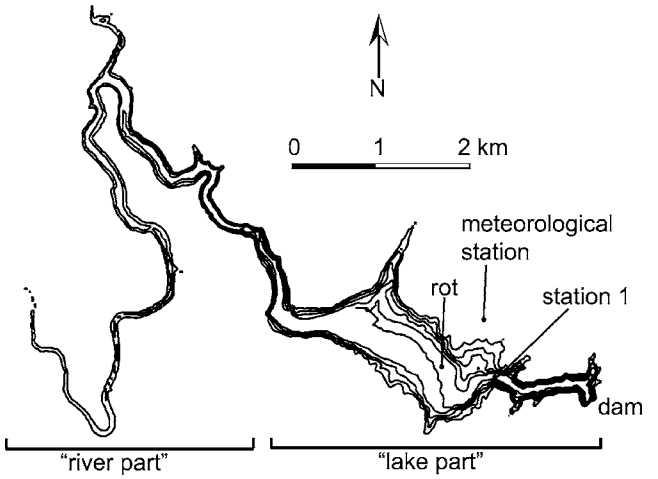

Fig. 1. Bathymetric map of the Sau reservoir showing the location of the measuring station, the meteorological station, the point selected for the rotational analysis (rot). The reservoir has been divided in two sections: "River part" and "lake part." The main axe of the "lake part" is oriented west northwest.

function (Münnich 1996, Fricker and Nepf 2000) shows that the V3H1 mode was an eigenvalue, with the same period as the wind. Therefore, resonance between the wind and the third mode was responsible for the excitation of this mode. Although internal Rossby radius estimations showed that rotational effects could be important, they were not taken into account in the two-dimensional model. The elongated shape of the reservoir led the authors to believe that the effect of the Kelvin mode is very similar to the effect that would have been caused by a mode without rotation and that the period of the Kelvin seiche should be almost identical to the seiche without rotation.

In this paper, we will demonstrate that in continuously stratified reservoirs, stratification together with the resonance with the wind forcing is the key factor in the selection of the predominant modes of oscillation of the reservoir. In the Sau reservoir, the vertical Modes V2 and V3 have been identified as the oscillation modes responding to the wind patterns of 12-h and 24-h periodicity. Model calculations show us that these periods are the corresponding natural periods of these modes. Therefore, the analogy between the reservoir and a forced damped oscillator is straightforward. In comparison, Mode V1 is much less important.

Methods

Sau is a canyon-shaped reservoir, 18.2 km long situated in the central part of the river Ter, which is 200 km long, with its source in the Pyrenees in the northeast of Spain (Armengol et al. 1999). The length of the widest part of the reservoir, called from now on, the "lake part," is 3.6 km and the maximum width is 1.3 km; the narrowest part of the reservoir will be called "the river part" (Fig. 1). Here, we present the results of different surveys carried out in the period July 2004–October 2004, during the stratification period of the reservoir.

An acoustic Doppler current meter (ADCP) and a thermistor string (TS) were deployed at station 1 (Fig. 1). The ADCP was active from July 20, 2004–August 4, 2004 and from September 7–9, and the TS from July 8–September 5 and from

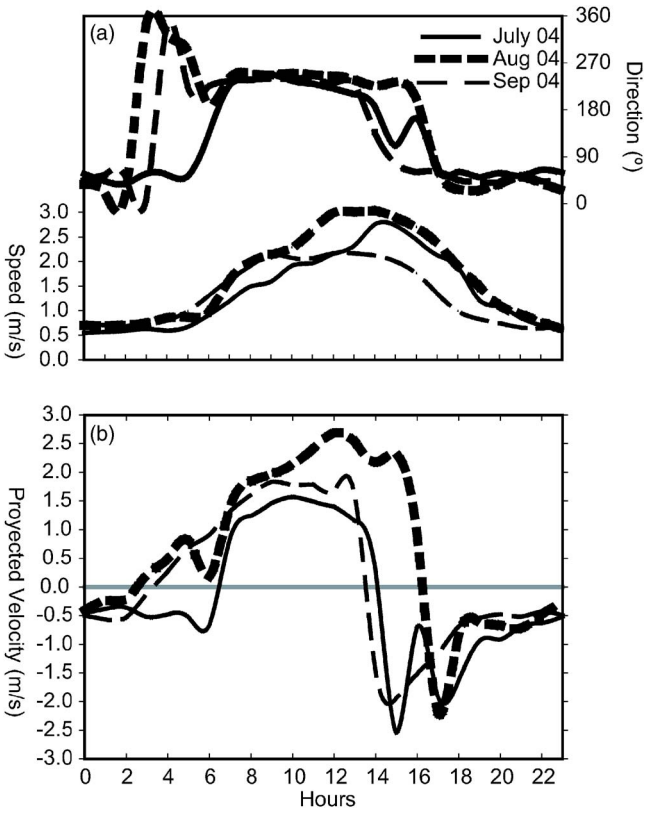

Fig. 2. (a) Summer averaged hourly values for the wind velocity and the wind direction. (b) Summer averaged hourly values for the wind velocity projected following the west northwest direction as indicated in Fig. 1.

September 9–October 9. Wind data were obtained from a meteorological station placed nearby the lake (Fig. 1).

The ADCP (RDI 600 kHz Workhorse Sentinel) was deployed near in the water surface and beaming downwards. Data from the ADCP were received from 55 depth bins, each 1 m thick, with the first bin at 2 m. The sampling rate was set at 1 Hz with the raw data processed to obtain 7.5 min averaged data, with a standard deviation of 0.1 cm s^{-1}. Speed-of-sound corrections due to the different temperatures in the water column were taken into consideration (Urick 1983), although in the worst case the introduced error by assuming constant sound speed was less than 4%. Between July 8–September 5, the available temperature records obtained with the TS were those at the following depths: 3, 4, 5, 6, 7, 8, 9, 11, 15, 16, and 17 m. Between September 9 and October 9 the depths of the sensors were changed to better fit the new stratification. At that time, the available temperature records were obtained at 8, 10, 11, 12, 13, 14, 16, 20, 21, 22, 27.5, 30, 32.5, and 37.5 m. There were no temperature data from September 5 to 9.

In addition to the experimental results, numerical simulations were carried out with the estuary and lake computer model (ELCOM). This model solves the 3D hydrostatic, Boussinesq, Reynolds-averaged Navier Stokes, and scalar transport equations, separating mixing of scalars and momentum from advection. Simulated processes include baroclinic and barotropic responses, rotational effects, wind stresses, surface thermal forcing, inflows, and outflows. For a model description, the reader is referred to Hodges (2000) and Hodges et al. (2000). Previous applications (Hodges et al. 2000; Laval et al. 2003; Gomez-Giraldo et al.

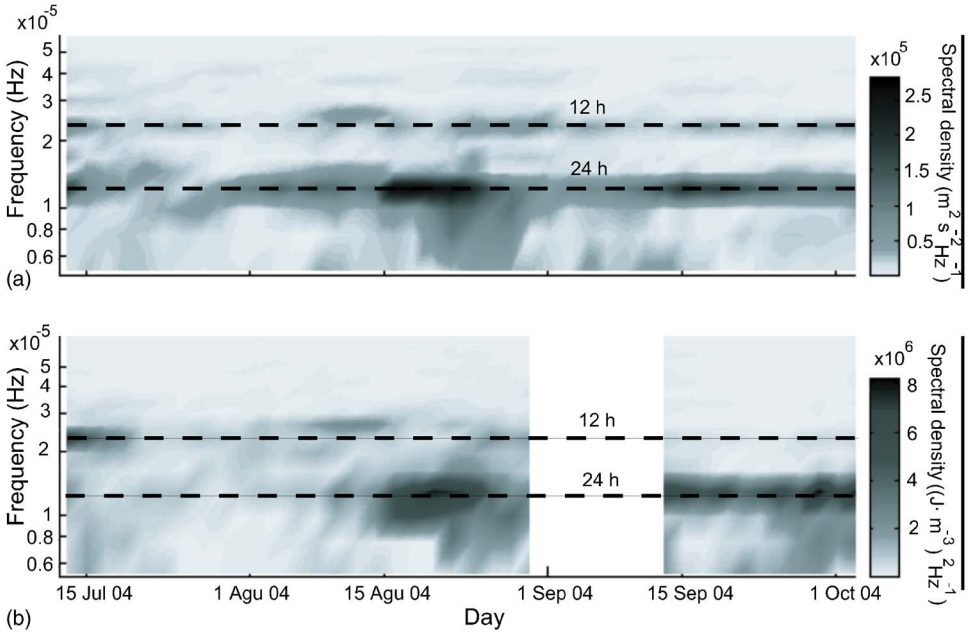

Fig. 3. (a) Evolution of the power spectra density for the projected wind velocity; (b) for the potential energy of volume of the water column (see the text)

2006) show that the model reproduces the internal wave field well in lakes, and, therefore, it is used to support our interpretation of the results.

For the application of the ELCOM model, the "river part" of Sau reservoir (Fig. 1) was straightened following Hodges and Imberger (2001), in order to decrease the numerical diffusion in that zone; the bathymetry was then discretized using a $35 \times 35 \times 1$ m grid and time steps of 45 s. To run the model, we used hourly mean meteorological data from the meteorological station indicated in Fig. 1. Wind was set to zero in the "river part" of the reservoir (Fig. 1), because here the reservoir is sheltered from the wind.

Results

In normal anticyclonic conditions, which are prevalent during summer, the daily wind pattern of the Sau reservoir is quite regular. During most of the day hours, the wind blows toward the dam, its direction being from 250° [Fig. 2(a)]. In the afternoon, wind changes direction to 70° (easterly) and blows upstream of the reservoir. Fig. 2(b) shows the projected wind velocity (monthly averaged) over the main axis of the reservoir. The highest values of the wind velocity are recorded prior to the change to easterly wind. The wind drops in the evening, but a slight breeze remains during the night. Fig. 2(b) shows a typical pattern for the wind conditions in the summer period. It has to be noted, however, that this pattern is disrupted when a front passes, although this is not very usual in summer time.

Power spectral density (PSD) describes how the power of a signal or time series is distributed with frequency (Antenucci et al. 2000; Lemmin 1987; Fotonoff 1969), and for such reason was selected in order to determine the main oscillations in Sau. Fig. 3(a) shows the evolution of the wind power spectral density for the stratified period of 2004. To compute the PSD on a specific day, a time series of 10 days centered on that particular day was used; we computed the PSD every two days from July 15, 2004 to October 1, 2004, and represented the contours in the figure. As in Fig. 2(b), the wind velocity has been projected following the main axis of the reservoir (Fig. 1). A dominant period of 24 h and a secondary, subdaily mode of 12 h periods can be clearly seen. The daily distribution in Fig. 2(b) suggests the dominance of the first two harmonics in the Fourier decomposition, corresponding to these periods. In a similar way, Fig. 3(b) shows the spectral density evolution of the potential energy per unit of volume calculated as

$$\mathrm{EP}(t) = \frac{1}{2} N^2(t) \rho_0(t) \xi^2(t) \tag{1}$$

where

$$N^2 = -\frac{g}{\rho_0} \frac{d\rho}{dz} \tag{2}$$

=buoyancy frequency; g=gravity acceleration; ρ=water density; and ξ=displacement of a selected isotherm. Values of N^2 and ρ_0 have been obtained from averaged values over the period in which the spectrum has been carried out. The selected isotherm has to be representative of the wave field of the system, and has been chosen as the temperature at the depth where the vertical displacements are higher. As its value changes with time, we have changed the isotherm approximately every 4 days, beginning with 19°C on July 15, increasing up to 22.5°C on August 31 and decreasing to 21°C on October 4. For both measured modes, the maximum vertical displacements occur at a depth of around 10 m, deepening slightly at the end of the summer. This depth roughly corresponds to the first layer's interface for both modes. In Fig. 3(b), it can also be seen that the 12 h and 24 h periods dominate the internal wave field; it will be seen later that these periods roughly correspond to forced V2 and V3 modes, respectively.

In Fig. 3(b), it can be seen that the same periods of 12 h and 24 h dominate the wave field in the second half of July and at the

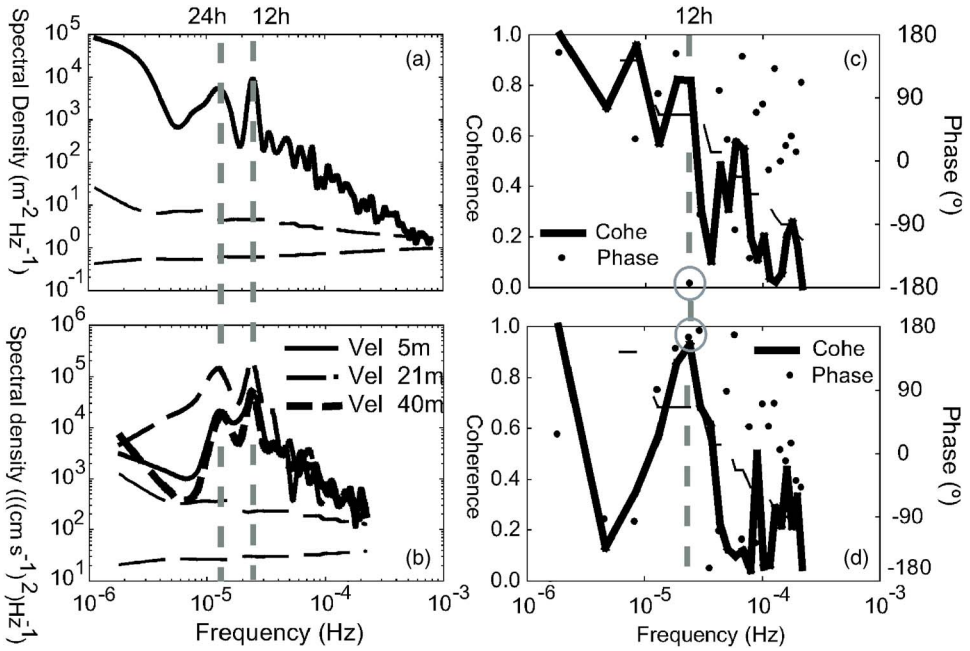

Fig. 4. (a) Power spectra density for the 19°C isotherm and (b) for the west northwest component of the velocity at different depths, for the period July 20, 2004–July 30, 2004. (c) Coherence and phase spectra for the projected velocities at 5 and 21 m and (d) for the projected velocities at 21 and 40 m depth. Spectra in (a) and (b) have been smoothed in the frequency domain to improve confidence. Dashed lines show confidence at 95% confidence. Vertical dashed lines show the periods corresponding to the maximum peaks.

end of September, respectively, coinciding with high spectral wind densities for the same modes. However, during the first two weeks of August, where the spectral density of the wind at 24 h is similar to that found in September [Fig. 3(a)], the 24-h response of the wave field is quite low [Fig. 3(b)]. Furthermore, in the last days of August, high spectral density is found at 24 h, in a period where the wind spectral density was the highest of the survey. All in all, it seems quite clear that the reservoir responds to the wind forcing by adjusting its frequency to that of the wind. However, the extent of the response will depend on the reservoir stratification. In the following sections, we will show that resonance between the wind and the internal modes of the reservoir will enhance this response.

Evidence of a V2 Mode

As has been shown in Fig. 3(b), at the end of July 2004, the 12-h period dominated the frequency spectrum for the temperature. This also can be seen by looking at the PSD for the 19°C isotherm [Fig. 4(a)]. From the ADCP data here, we will use velocity spectra to demonstrate the existence of a V2 oscillating mode. The spectral analysis for the velocity at different selected depths (5, 21, and 40 m) show a dominant mode around 12 h, despite the existence of the 24-h oscillation as a consequence of the main wind periodicity [Fig. 4(b)]. Furthermore, the velocity at 5 m depth and the velocity at 21 m depth oscillate in opposite phase [Fig. 4(c)], and the velocity at 21 m and velocity at 40 m also oscillate in opposite phase [Fig. 4(d)]. This indicates the existence of three layers oscillating each one in opposite phase, as is characteristic of the V2 mode.

Additional proof of the presence of the V2 mode comes from the observation of the velocity field obtained with the ADCP [Fig. 5(a)], after passing a bandpass filtered velocity over a period of 12±1.2 h [Fig. 5(b)]; the three-layered structure is clearly appreciated corresponding to the V2 mode. Note that the maximum and minimum vertical displacements of the inferred isotherms (solid lines) take place when water velocity reverses its direction, as expected from the standing internal wave behavior for the Mode V2. Fig. 5(c) shows the averaged vertical temperature profile at Station 1 on July 20, 2004.

Evidence of a V3 Mode

The vertical displacement of three selected isotherms (22, 13.5, 8.5°C) in September 2004 shows that there is a predominant oscillation of 24 h, coinciding with the wind period [Fig. 6(a)]. This is especially clear from September 19, 2004 [day 9 in Fig. 6(a)] onwards. Furthermore, the 22°C isotherm oscillation is in the opposite phase with the 13.5°C isotherm and in phase with the 8.5°C isotherm [see dotted lines in Fig. 6(a)], indicating the presence of three vertical displacements and, therefore, a V3 mode. Note that in Fig. 6(a), the vertical displacement scale for the different isotherms is not the same.

Fig. 6(b) shows two temperature profiles measured within 12 h difference, that is, half of the oscillation period, approximately when the maximum displacements are found [see dotted lines in Fig. 6(a)] on September 22. The three vertical displacements, together with the layer structure of the V3 mode, are appreciated in Fig. 6(b). Note that the minimum vertical displacements correspond to the intermediate layer (13.5°C isotherm), where the temperature gradient is maximum and the stability higher. The presence of the V3 mode can be corroborated by making the spectral analysis of the isotherm time series for the three selected isotherms, where the 24-h peak is clearly enhanced [Fig. 7(a)]. In addition, in the 24-h peak, the 22°C and 13.5°C isotherms are coherent, but oscillate in the opposite phase [Figure 7(b)]. Furthermore, the 13.5°C isotherm oscillates in opposite phase with the 8.5°C isotherm [Figure 7(c)], indicating that each one of the

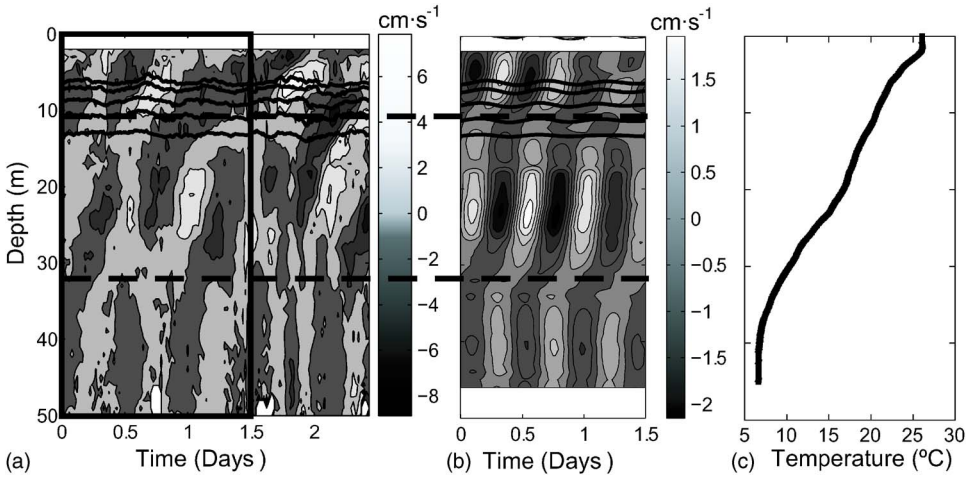

Fig. 5. (a) Projected velocity obtained with the ADCP at Station 1 and (b) using a 12 h band-pass filter. Day 0 corresponds to July 27, 2004; dashed lines show the three-layer structure. (c) Averaged temperature profile at Station 1 on July 20, 2004.

three vertical oscillations are in opposite phase with the next. As the coherent oscillation that can be appreciated in the 12-h peak, for the 22, 13.5, and 8.5°C isotherms [see Figs. 7(b and c)], corresponds to a very low spectral density [Fig. 7(a)], no further analysis has been carried out.

Model Results

Mode V2

Model results reproduce the modal envelope quite well and the predicted periods for the oscillation of the V2 mode occurring in July 2004. Fig. 8 shows the good agreement between the modeled and the measured velocity field at Station 1 (Fig. 1) for the last days of July. Notice that the changes of direction in the velocity are almost identical in the model and the ADCP data. Fig. 9 shows the horizontal structure of the V2 mode predicted by ELCOM for the July survey for the three selected isotherms: 21.5, 20, and 10°C. The results in Fig. 9 correspond to July 20, 2004. The model was initialized 4 days before and the applied wind field over the lake was the measured wind at the meteorological station (Fig. 1). Inflows and outflows were also simulated; however, during the simulated period, the inflow rate was quite low (around 2 $m^3 s^{-1}$) and the outlet structures were closed, so they do not have much relevance in the internal wave field. The 12 h oscillation reproduced by the model embraces the entire reservoir as a basin-scale internal wave and is observed in both the "lake part" and the "river part" of the reservoir. Note that the isotherms 21.5 and 20°C (layers located at approximately 8 m and 12 m, respectively), oscillate in opposite phase with the isotherm of 10°C (layer located at 30 m), corresponding with the V2 mode. Due to the cutoff of the current in the deepest layer, the structure of this mode is not simple. While the typical structure of a V2 mode can be appreciated in the main body of the reservoir, in the river part the layers oscillate in phase.

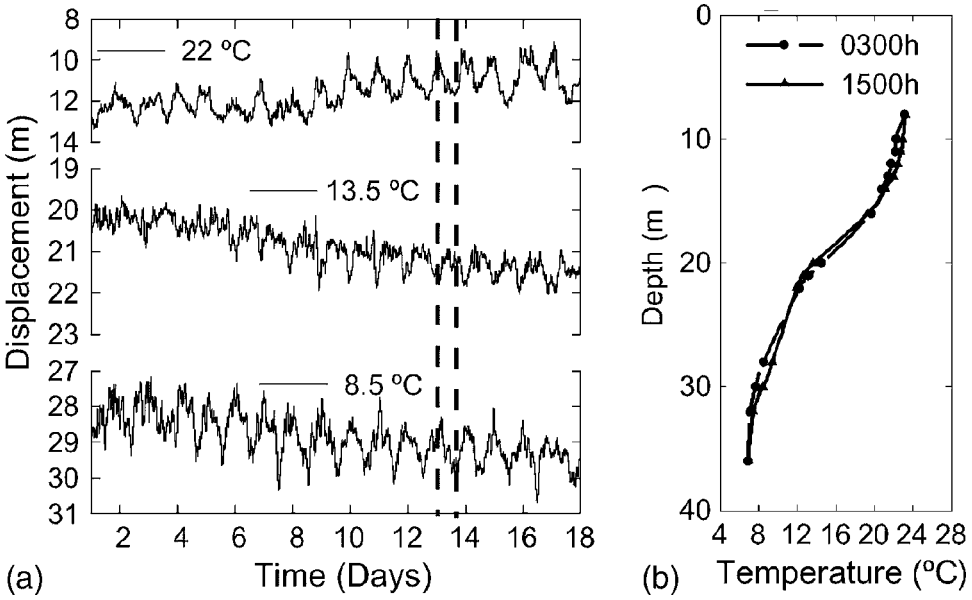

Fig. 6. (a) Isotherm vertical displacements at Station 1. Day 0 corresponds to September 10, 2004. Dotted lines show the experimental evidence for the Mode V3. (b) Temperature profiles at two different hours measured with the thermistor string at Station 1 on September 22, 2004.

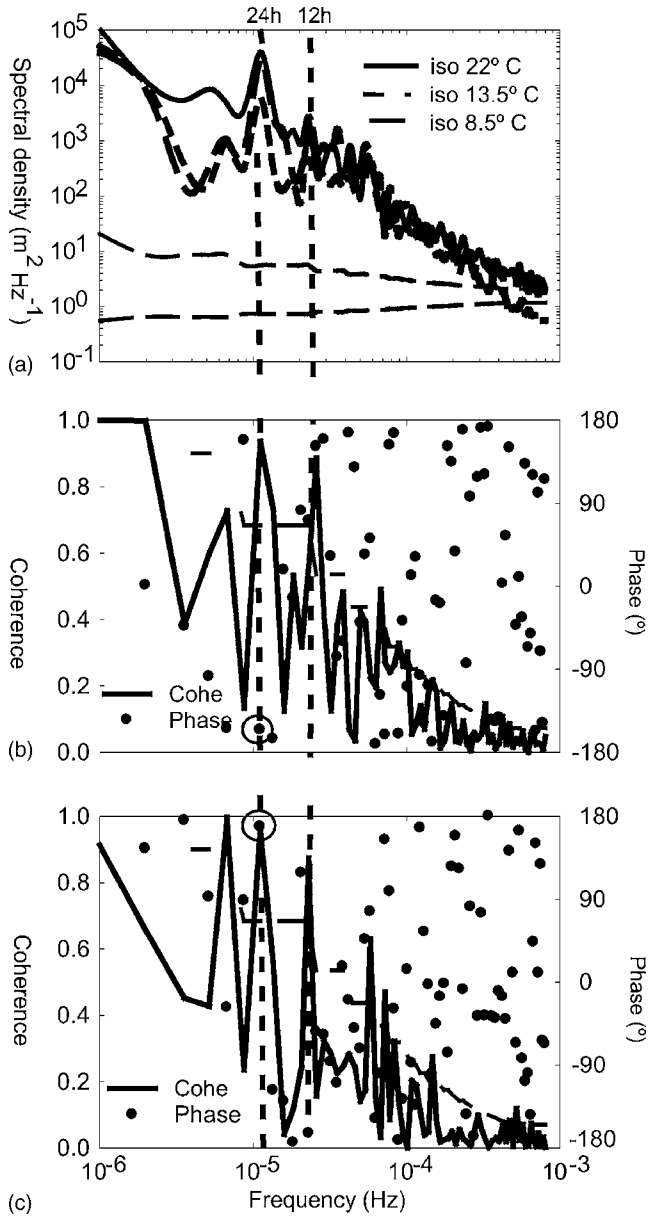

Fig. 7. (a) Power spectra densities for three selected isotherms for the period September 18–28, 2004; spectra have been smoothed in the frequency domain to improve confidence; dashed lines show confidence at the 95% level. (b) Coherence and phase spectra for 22 and 13.5°C isotherms. (c) Coherence and phase spectra of isotherms 13.5 and 8.5°C. Dashed lines show confidence at the 95% confidence. Vertical dashed lines show the periods corresponding to the maximum peaks.

Mode V3

Comparison of the model results with experimental data for September at Station 1 (Fig. 1) reveals generally good accuracy. In Fig. 10(a), the vertical displacements of three selected isotherms (22, 16, and 8.5°C) are compared with those obtained with ELCOM, during a 7-day period. It can be seen that the experimental and the modeled results for the 22°C isotherm begin to diverge after 4 days. As this isotherm is situated at the bottom of the surface mixing layer [Fig. 6(b)], and mixing in this zone is very active, we expect, therefore, that the model diverges sooner than in the other zones. In fact, small differences in the turbulent kinetic energy budget could cause the displacement of the isotherm, rather than the internal wave dynamics. The fact that ELCOM underestimates the vertical displacements can be attributed to the artificial dissipation introduced by the nonnormal flow boundary condition applied on the lake bottom discretization. This underestimation is even clearer for the case of Lake Kinneret (Gomez-Giraldo et al. 2006). The predicted and simulated spectral densities for the 16 and 8.5°C isotherms at Station 1 [Figs. 10(b and c)] show also the dominance of the 24-h period. The smallest scales are not obviously well resolved by the model and because of this, real and simulated values diverge at frequencies lower than $\sim 10^{-4}$ Hz.

Fig. 11 shows the horizontal structure of the V3 mode, affecting the entire reservoir, as predicted by ELCOM during a 24-h cycle at intervals of 6 h (that is, at every quarter of the period) for the three selected isotherms (22, 16, and 8.5°C). Fig. 11(A) corresponds to September 20 at 15:00 h. The model was initialized 4 days before and the forcing wind was that measured at the meteorological station (Fig. 1); as before, the river inflow was very low and the outlets were closed; therefore, they were not relevant for the internal wave field. Unfortunately, we have no field data from stations other than Station 1 to compare with the model results. However, the good agreement obtained at this station makes us think that the model can be useful to simulate the horizontal structure of the Sau reservoir. In addition, in a previous survey (Vidal et al. 2005), it was shown that the shallower layers at a station placed at the intersection between the "lake part" and the "river part" (Fig. 1), oscillated in the opposite phase to the shallower layers at Station 1, in agreement with model results predicted in Fig. 11.

In Figs. 11(A) and 11(C), the vertical displacements are maximum and opposite each other. Fig. 11(E) schematizes Fig. 11(C), following the thalweg and exaggerating the vertical displacements, in order to appreciate the nodal lines. As there are two sets of three nodal lines, the oscillation mode would be a V3H2 instead of a V3H1, as was predicted in Vidal et al. (2005), where only the "lake part" was considered. It has to be noted, however, that the V*n*H*m* classification for the modes applies to a rectangular basin and loses meaning when the shape is different from that. In Fig. 11, it can also be seen how the nodal lines are displaced towards the dam in the deepest isotherms. In the river part of the reservoir, the vertical displacements are also smaller. This is to be expected, because internal waves originate from the wind field in the "lake part" of the reservoir. When they travel to the "river part," where the wind velocity was set to zero, dissipation increases. This penetration in the sloping "river part" can cause wave breaking and shear-induced convective mixing (Boegman et al. 2005; Lorke et al. 2005), also increasing the mixing in the river inflow.

Rotational effects are not negligible in the main body of the Sau reservoir. By looking at Fig. 11, an anticlockwise rotation in the upper layer (isotherm 22°C) can be observed; however, in the deeper layer (isotherm 8.5°C) the rotation is negligible. This fact is better clarified by looking at the rotational spectrum (Gonella 1972) of both layers, carried out using model data from the point marked as "rot" in Fig. 1, where rotational effects could be expected (Fig. 12). A 24-h anticlockwise oscillation for the isotherm 22°C is observed [Fig. 12(a)], although some clockwise components of the spectra indicate the elliptical shape of the rotation. For the isotherm 8.5°C [Fig. 12(b)], both components (clockwise and anticlockwise) are almost identical, indicating a linear oscillation. In fact, in the upper layer, the Rossby radius $\mathrm{ro}=c/f$, where c is the phase speed of the internal wave and f the Coriolis parameter, can be estimated as follows. The phase speed will be

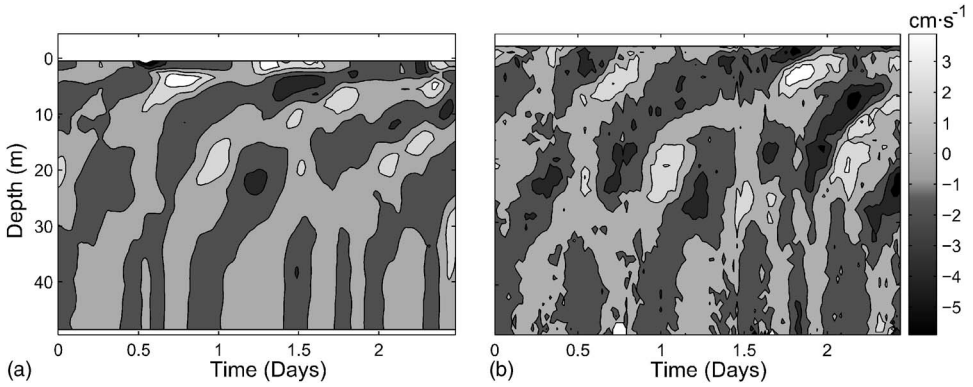

Fig. 8. (a) Projected velocity comparison between ELCOM and (b) measured ADCP data at Station 1. Day 0 corresponds to July 27, 2005.

λ/T, where T is 24 h and λ=wavelength of the 22°C isotherm following the thalweg, which is $\lambda \approx 8$ km (see Fig. 11) and f is 1.02×10^{-4}; therefore, ro≈0.9 km, similar to the width of the reservoir, which is also around 0.9 km for that isotherm.

Natural Modes

Given the good description obtained with ELCOM for the Sau reservoir, the next step is to use the model to calculate the period for the natural modes of oscillation. In order to undertake this task, we run the model without external forcing, i.e., with no meteorological inputs, inflows, or outflows. We also chose the temperature with tilted isotherms represented in Fig. 9 as the initial spatial condition, corresponding with the excited V2 mode on the 20th of July. These isotherms correspond to the maximum vertical displacements, band-pass filtered over a 12 h period, obtained when ELCOM was used to simulate this mode (see Model Results). However, in that case, the wind was forcing the mode; but now, by setting the wind to zero we expect to obtain the natural period of the mode. Similarly, we used the isotherms represented in Fig. 11(A) as the initial condition for the V3 mode on the 20th of September. The natural period of every mode was then calculated by fitting a selected isotherm oscillation in a particular location (we chose Station 1) to a damping sinusoidal function [see Gomez-Giraldo et al. (2006) for the details]

$$X_i(t) = A \times e^{-\alpha t} \times \sin(\omega t) \tag{3}$$

where $X_i(t)$=vertical displacement of the i selected isotherm (at the pycnocline) at time t; A=initial amplitude, and α=inverse of the e-folding time. ω and ω_0=damped and undamped natural frequencies, respectively, related by the equation:$\omega^2=\omega_0^2-\alpha^2$. Parameters A, α, and ω for the simulated oscillation are then obtained by least-squares fitting. As high frequency oscillations tend to appear due to internal wave degeneration, a low-pass filter was previously applied to the isotherm in order to improve the fitting process. The filter cutoff was 9 h for the V2 mode and 20 h for the V3 mode. Finally, the natural damped periods obtained with the model were 25.5 h for the V3 mode on the 20th of September and 12.3 h for the V2 mode on the 20th of July, and since they were close to 24 and 12 h, respectively, resonance may occur in those periods.

Now we will demonstrate how the Sau reservoir behaves as a forced oscillator. Forced oscillation theory shows that, after a certain period of time where transient effects can occur, the resultant frequency follows the forcing frequency. When damping is small and the forcing frequency is close to one of the natural frequencies of the oscillator, resonance takes place and the amplitudes are high. We will use the model ELCOM to simulate the reservoir response to an idealized forcing wind characterized by a west northwest wind speed $v_{wind}=v_o \cos \omega t$, where v_o is 3 m s^{-1}. The angular frequency will be varied from periods of 5 to 24 h with 1 h interval. The selected initial stratification will correspond to the temperature profile taken on the 20th of July [Fig. 5(c)] with the reservoir horizontally homogeneous. In this case, the stratification (buoyancy frequency N) was almost constant with depth, guaranteeing that all the modes can be equally excited. The model was run for a 10-day period, and the results were analyzed using spectral analysis.

Fig. 13 shows the power spectral density (PSD_M) of vertical displacements integrated for the whole water column at Station 1 as obtained by ELCOM for the different wind forcing periods. (For the sake of clarity, we use forcing periods instead of forcing frequencies). That is

$$PSD_M = \frac{1}{H}\int_0^H PSD_{isotherm}(z)dz \tag{4}$$

where H=total depth; $PSD_{isotherm}(z)$=power spectral density of the vertical motions of the isotherm at the depth z; and dz=discretized to 1 m increments. Fig. 13 shows that for each forcing period, the PSD_M is maximum coinciding with the period of the forcing wind. Furthermore, maximum values of PSD_M are found in 6 h, 12–13 h, and 19–20 h (marked with circles in the figure). We should expect that these maximum values correspond

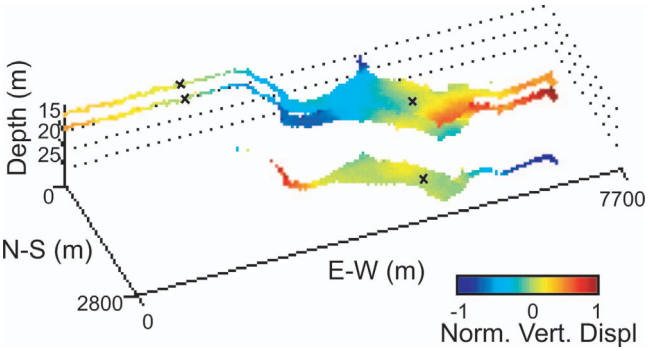

Fig. 9. (Color) Evolution of the ELCOM predicted vertical displacement for the 21.5, 20, and 10°C isotherms; normalized [−1 1] and 12 h band-pass filtered, corresponding to day July 20, 2004. Crosses show the approximate position of the nodal points in the horizontal structure.

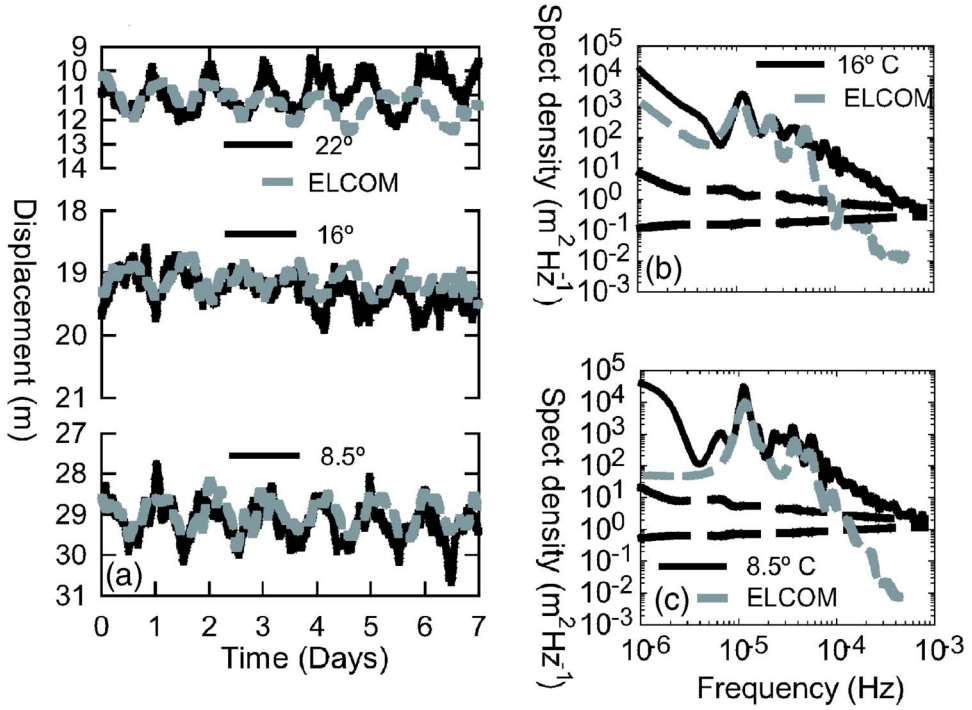

Fig. 10. (a) Vertical displacement for three selected isotherms obtained with the thermistor string (black line) and ELCOM model (gray line) at Station 1. Day 0 corresponds to September 20, 2004; (b) power spectral density comparison between measured and predicted temperatures for the period September 20–28, 2004 for the 16°C isotherm; and (c) for the 8.5°C isotherm.

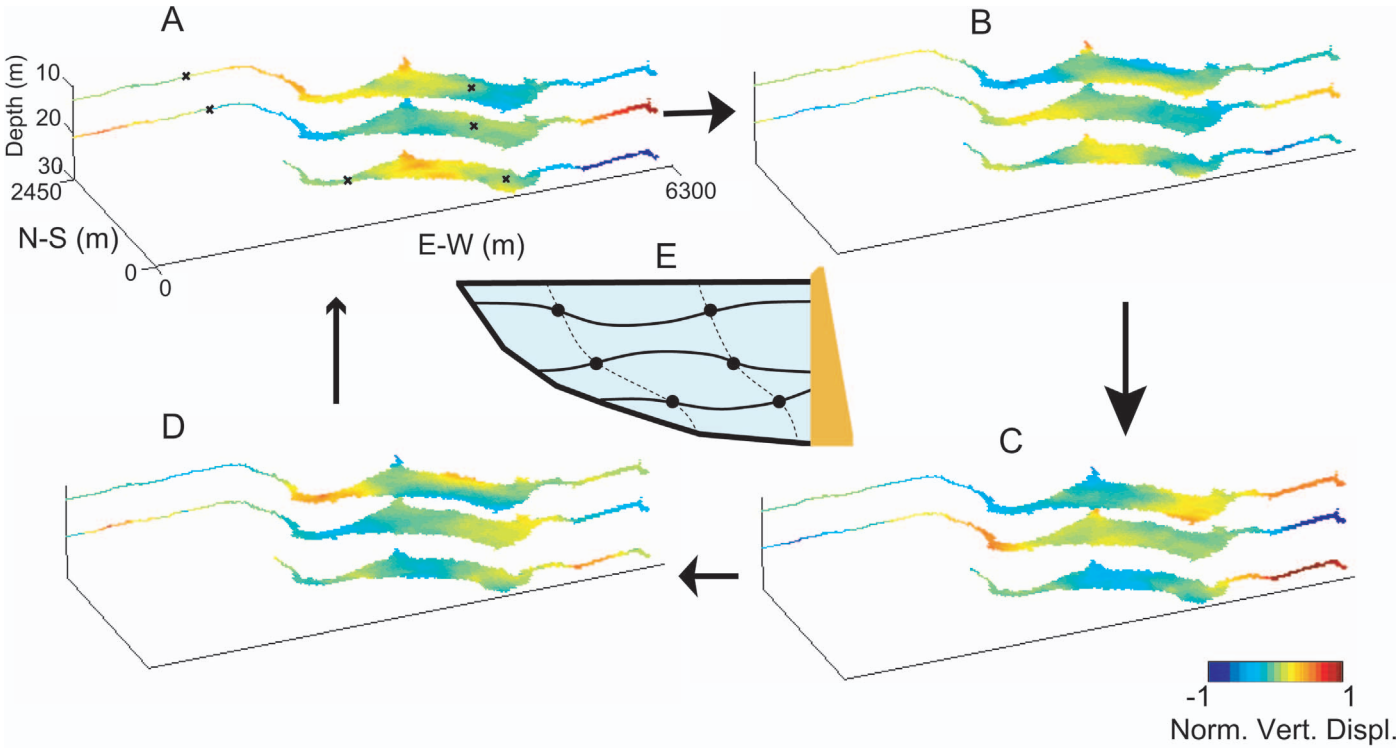

Fig. 11. (Color) (A)–(D) Evolution of the ELCOM predicted vertical displacement of the 22, 16, and 8.5°C isotherms at intervals of 6 h, normalized [−1 1] and 24 h band-pass filtered corresponding to day September 20, 2004. (E) Sketch of the vertical structure corresponding to (C), following the thalweg, exaggerating the vertical displacements, and showing the nodal points. Crosses in (A) show the approximate position of the nodal points in the horizontal structure.

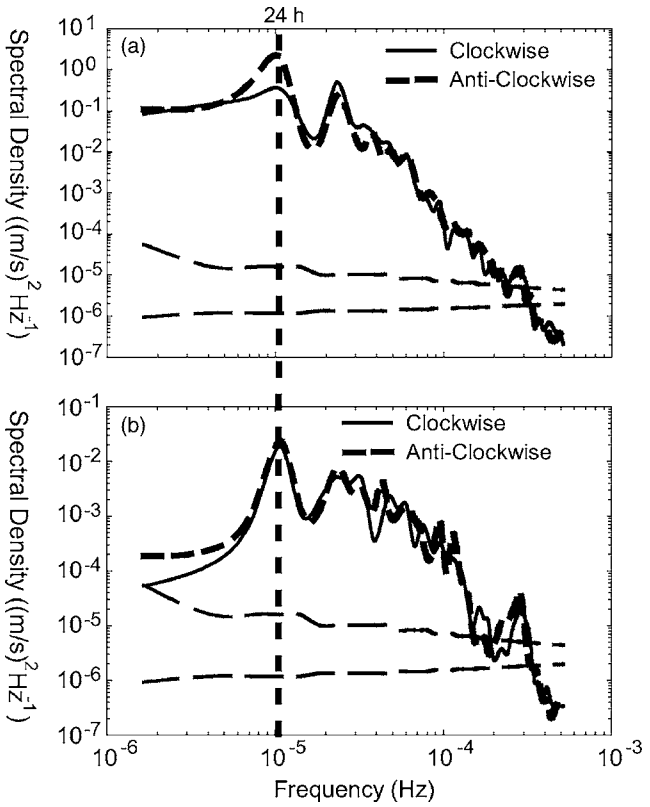

Fig. 12. (a) Rotary spectra of horizontal currents, decomposed into clockwise and anticlockwise rotating components at the 22°C isotherm depth; (b) at the 8.5°C isotherm depth obtained with ELCOM model at the point "rot" (Fig. 1). Dashed lines show confidence limits at the 95% level with spectra smoothed in the frequency domain to improve confidence. The peak frequency corresponding to period of 24 h is shown.

to resonant periods where vertical displacements are amplified. Visual inspection of the oscillation dynamics for each period shows that the maxima roughly correspond to the Modes V1, V2, and V3. The displacement of the isotherms shows the existence of one vertical displacement, as expected for the Mode V1, with a forcing period of 6 h [Fig. 14(a)], two vertical displacements for the Mode V2, with a forcing period of 12 h [Fig. 14(c)], or three vertical displacements for the Mode V3, with a forcing period of 19 h [Fig. 14(d)]. Furthermore, for an intermediate period between two maxima as 8 h [Fig. 14(b)], the response of the reservoir is not an organized motion, with smaller displacements, as expected in nonresonant periods.

Discussion

While there are periods where the existence of the vertical Modes V2 and V3 is clearly seen (Figs. 5 and 6), there are others, for example in early August (see Fig. 3), where vertical displacements are smaller and the spectral peaks are not so pronounced. Nevertheless, the response of the reservoir to wind forcing also shows predominant frequencies of 24 and 12 h (Fig. 3), although now the reservoir response is probably due to the direct effect of the wind, rather than to internal waves. We hypothesize that in this case, the stratification does not allow a mode with a similar period as the wind forcing and, therefore, the energy transfer to

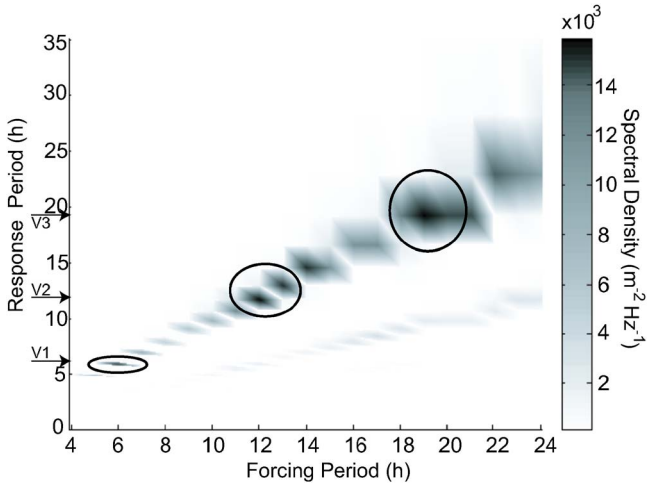

Fig. 13. Contours of the power spectral density (PSD_M) of vertical isotherm displacements integrated for the whole water column at Station 1 as obtained with ELCOM for the different wind forcing periods. Circles and arrows in the y axis indicate when a forcing period coincides with the natural oscillation Modes V1, V2, and V3 calculated with ELCOM. Stratification is taken from July 20 when the buoyancy frequency $N(z)$ was nearly constant with depth.

internal waves is much smaller. Estimations made with ELCOM corroborate that the period of oscillation for the Modes V2 and V3 is in this case different from 12 and 24 h.

The periods of the natural Modes V1, V2, and V3, for the 20th of July can also be obtained by rerunning ELCOM without the wind forcing. In this case the initial tilting of the isotherms has been deduced from the temperature profiles obtained in the previous runs of the model, where the position of the layers can be inferred. The corresponding natural periods are 5.8 h for V1, 12.3 h for V2, and 19.7 h for V3, very similar to the periods where maximum values of PSD_M are obtained (see Fig. 13).

Therefore, given the initial stratification corresponding to July 20, 2004, if the reservoir is forced by winds of periods 6, ~12, or ~19 h, maximum values of PSD_M are obtained indicating the existence of resonance between the wind and the internal wave field. Given that the wind field at mid-July shows two main forcing frequencies, corresponding to the harmonics 24 and 12 h [Fig. 3(a)], and that the natural frequency of the Mode V2 is close

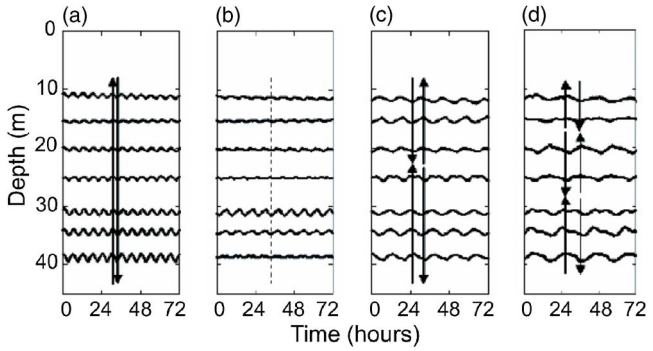

Fig. 14. (a) Isotherm evolution obtained with ELCOM for a wind forcing period of 6 h; (b) 8 h; (c) 12 h; and (d) 19 h. Arrows indicate the vertical displacement for two opposite estates corresponding to Modes V1 in (a); V2 in (c); V2 and V3 in (d).

to 12 h, it can be expected that this would be the chosen oscillation mode, as in fact occurs, as shown previously.

We can conclude by remarking that, at larger scales, the Sau reservoir behaves as a forced oscillator. It responds to the periodic winds of 12 and 24 h with water movements of the same period. However, when stratification allows one of the natural periods of the reservoir to be close to the forcing period, the energy transfer from the wind is higher because of the resonance. This happens in mid-July for the Mode V2 and in mid-September for the Mode V3. The model ELCOM shows that the structure of the Mode V3 presents two horizontal nodal lines. The Mode V2, instead, has two horizontal nodal lines at the surface but only one at the bottom. Both modes are affected by the Earth's rotation in the widest part of the reservoir, where amphidromies are formed. It also has to be noted that at the latitude of the reservoir, the diurnal and semidiurnal periods are 35.2 and 17.6 h, respectively, both of which are far from the forcing frequency.

Acknowledgments

This work was supported by the Spanish government (MEC) through the CGL2004-02027/HID project. The writers thank the Catalan Water Agency and Aigües Ter-Llobregat for their support throughout the field campaigns. The writers thank the Center for Water Research (CWR-UWA), and its director Jörg Imberger for providing the writer with the model ELCOM, and also to Sebastian Morillo and Andres Gomez-Giraldo for their help in the use of it. The writers also thank Joan Armengol for his encouragement in the study of the Sau reservoir.

References

Antenucci, J. P., and Imberger, J. (2003). "The seasonal evolution of wind/internal wave resonance in Lake Kinneret." *Limnol. Oceanogr.*, 48, 2055–2061.

Antenucci, J. P., Imberger, J., and Saggio, A. (2000). "Seasonal evolution of the basin scale internal wave field in a large stratified lake." *Limnol. Oceanogr.*, 45, 1621–1638.

Armengol, J., et al. (1999). "Longitudinal processes in canyon type reservoir: The case of Sau (N.E. Spain)." *Theoretical reservoir ecology and its applications*, J. G. Tundisi and M. Straskraba, eds., Backhuys, The Netherlands, 313–345.

Boegman, L., Ivey, G. N., and Imberger, J. (2005). "The degeneration of internal waves in lakes with sloping topography." *Limnol. Oceanogr.*, 50, 1620–1637.

Fotonoff, N. P. (1969). "Spectral characteristics of internal waves in the ocean." *Deep-Sea Res.*, 16 (supp), 58–71.

Fricker, P. D., and Nepf, H. M. (2000). "Bathymetry, stratification, and internal seiche structure." *J. Geophys. Res.*, 105, 14237–14251.

Gaedke, U., and Schimmele, M. (1991). "Internal seiches in Lake Constance: Influence on plankton abundance at a fixed sampling site." *J. Plankton Res.*, 13(4), 743–754.

Gloor M., Wüest, A., and Münnich, M. (1994). "Benthic boundary mixing and resuspension induced by internal seiches." *Hydrobiologia*, 284, 59–68.

Gómez-Giraldo, A., Imberger, J., and Antenucci, J. P. (2006). "Spatial structure of the dominant basin-scale internal waves in Lake Kinneret." *Limnol. Oceanogr.*, 51, 229–246.

Gonella, J. (1972). "A rotary-component method for analyzing meteorological and oceanographic vector time series." *Deep-Sea Res.*, 19, 833–846.

Hodges, B. R. (2000). "Numerical techniques in CWR-ELCOM." *Technical Rep. Ref. No. WP 1422-BH*, Centre for Water Research, Univ. of Western Australia, Nedlands, Western Australia.

Hodges, B. R., and Imberger, J. (2001). "Simple curvilinear method for numerical methods of open channels." *J. Hydraul. Eng.*, 127(11), 949–958.

Hodges, B. R., Imberger, J., Saggio, A., and Winters, K. (2000). "Modeling basin-scale internal waves in a stratified lake." *Limnol. Oceanogr.*, 45, 1603–1620.

Kamykowski, D. (1979). "The growth response of a model *Gymnodinium splendens* in stationary and wavy water columns." *Mar. Biol. (Berlin)*, 50, 289–303.

Laval, B., Imberger, J., Hodges, B., and Stoker, R. (2003). "Modeling circulation in lakes: Spatial and temporal variations." *Limnol. Oceanogr.*, 48, 983–994.

LaZerte, B. D. (1980). "The dominating higher order vertical modes of the internal seiche in a small lake." *Limnol. Oceanogr.*, 25, 846–854.

Lemmin, U. (1987). "The structure and dynamics of internal waves in Baldeggersee." *Limnol. Oceanogr.*, 32, 43–61.

Lemmin, U., Mortimer, C. H., and Baüerle, E. (2005). "Internal seiche dynamics in Lake Geneva." *Limnol. Oceanogr.*, 50, 207–216.

Levy, D. A., Johnson, R. L., and Hume, J. M. (1991). "Shifts in fish vertical distribution in response to an internal seiche in a stratified lake." *Limnol. Oceanogr.*, 36, 187–192.

Lorke, A., Peeters, F., and Wüest, A. (2005). "Shear-induced convective mixing in bottom boundary layers on slopes." *Limnol. Oceanogr.*, 50, 1612–1619.

McManus, M. A., et al. (2005). "Effects of physical processes on structure and transport of thin zooplankton layers in the coastal ocean." *Mar. Ecol.: Prog. Ser.*, 301, 199–215.

Münnich, M. (1996). "Influence of bottom topography on internal seiches in stratified media." *Dyn. Atmos. Oceans*, 23, 257–266.

Münnich, M., Wüest, A., and Imboden, D. M. (1992). "Observations of the second vertical mode of the internal seiche in an alpine lake." *Limnol. Oceanogr.*, 37, 1705–1719.

Pahl-Wostl, C., and Imboden, D. (1990). "Dyphora—A dynamic model for the rate of photosynthesis of algae." *J. Plankton Res.*, 12, 1207–1221.

Roget, E., Salvadé, G., and Zamboni, F. (1997). "Internal seiche climatology in a small lake where transversal and second vertical modes are usually observed." *Limnol. Oceanogr.*, 42, 663–673.

Spiegel, R. H., and Imberger, J. (1980). "The classification of mixed layer dynamics in lakes of small to medium size." *J. Phys. Oceanogr.*, 10, 1104–1121.

Stevens, C., Lawrence, G., Hamblin, P., and Carmack, E. (1996). "Wind forcing of internal waves in a long narrow stratified lake." *Dyn. Atmos. Oceans*, 24, 41–50.

Urick, R. J. (1983). *Principles of underwater sound*, 3rd Ed., McGraw-Hill, New York.

Vidal, J., Casamitjana, X., Colomer, J., and Serra, T. (2005). "The internal wave field in Sau reservoir: Observation and modeling of a third vertical mode." *Limnol. Oceanogr.*, 50, 1326–1333.

Wiegand, R. C., and Chamberlain, V. (1987). "Internal waves of the second vertical mode in a stratified lake." *Limnol. Oceanogr.*, 32, 29–42.